JACS Au
AN OPEN ACCESS JOURNAL OF THE AMERICAN CHEMICAL SOCIETY

pubs.acs.org/jacsau
Article

Conversion of Methane at Room Temperature Mediated by the Ta−Ta σ-Bond

Qian Li, Qing-Yu Liu,* Yan-Xia Zhao,* and Sheng-Gui He

Cite This: *JACS Au* 2024, 4, 1824−1832
Read Online

ACCESS | Metrics & More | Article Recommendations | Supporting Information

ABSTRACT: Metal−metal bonds constitute an important type of reactive centers for chemical transformation; however, the availability of active metal−metal bonds being capable of converting methane under mild conditions, the holy grail in catalysis, remains a serious challenge. Herein, benefiting from the systematic investigation of 36 metal clusters of tantalum by using mass spectrometric experiments complemented with quantum chemical calculations, the dehydrogenation of methane at room temperature was successfully achieved by 18 cluster species featuring σ-bonding electrons localized in single naked Ta−Ta centers. In sharp contrast, the other 18 remaining clusters, either without naked Ta−Ta σ-bond or with σ-bonding electrons delocalized over multiple Ta−Ta centers only exhibit molecular CH_4-adsorption reactivity or inertness. Mechanistic studies revealed that changing cluster geometric configurations and tuning the number of simple inorganic ligands (e.g., oxygen) could flexibly manipulate the presence or absence of such a reactive Ta−Ta σ-bond. The discovery of Ta−Ta σ-type bond being able to exhibit outstanding activity toward methane conversion not only overturns the traditional recognition that only the metal−metal π- or δ-bonds of early transition metals could participate in bond activation but also opens up a new access to design of promising metal catalysts with dual-atom as reactive sites for chemical transformations.

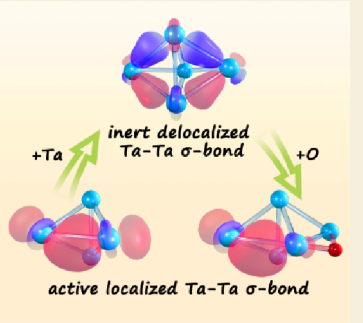

KEYWORDS: *C−H activation, Ta−Ta σ-bond, ligand effect, mass spectrometry, quantum chemical calculations*

1. INTRODUCTION

Transition metals feature the advantages of tunable electronic configurations and diverse oxidation states, thus being extensively used as powerful redox catalysts for upgrading abundant methane into liquid fuels and valuable chemicals, the reactions of which are of paramount importance to mitigate energy crisis and greenhouse effect.[1−4] However, due to the inherent inertness of the CH_4 molecule with a strong C(sp^3)−H bond, high ionization energy, low proton affinity, and negligible electron affinity, the availability of efficient transition metal catalysts that are active enough to bring about methane conversion under mild conditions remains a serious challenge. Substantial efforts have been devoted to the design of active metal sites with unique structural characteristics to achieve methane activation and subsequent transformation at low temperatures. An outstanding example is single-atom catalysts with single metal atoms (e.g., Rh,[5,6] Au,[7] Fe,[8] Co,[9] Ni[10]) stably anchored on suitable supports. In fact, in addition to single metal atom sites, the cooperativity between metal atoms in close proximity has also been developed as a promising strategy for catalyzing a wide variety of homogeneous organic reactions,[11−17] benefiting from the tunable features of metal−metal bonds such as bond order and polarity, harnessed by ligand modification. However, the employment of metal−metal cooperation to tackle the challenging chemistry of methane activation and conversion has rarely been achieved so far. It is highly desirable to establish a structural basis of the metal−metal bonds that are advantageous for C−H activation and to understand how to fine-tune metal−metal cooperativity to benefit methane conversion at room temperature.

Metal−metal bonds are ubiquitous in atomic clusters composed of multiple metal atoms, which provide an excellent platform to explore the critical role of metal−metal interaction displayed in activation and transformation of inert molecules. With the development of experimental techniques (e.g., laser vaporization) for preparation of metal clusters in isolated gas-phase environments, the reactivity of transition metal clusters toward methane has gained great attention in the area of cluster science since 1980s.[18−28] A considerable number of bare noble metal (NM) clusters in different charge states (e.g., $Pd_{n\le23}$,[29] $Pt_{n\le24}^{\pm}$,[30] $Rh_{n\le10}^{-}$[31]) were observed to dehydrogenate methane at room temperature. Available mechanistic studies revealed that single NM atoms generally serve as reactive sites to bring about C−H activation. By contrast, the investigations about bare transition metal clusters without NM atoms (e.g., $Co_{n\le22}^{+}$,[32] $Fe_{n\le15}^{+}$,[33] $Ni_{n\le16}^{+}$,[34] and $Cu_{n\le4}^{+}$[35]) showed that most of the nonprecious metal atoms are

Received: January 9, 2024
Revised: April 3, 2024
Accepted: April 4, 2024
Published: April 18, 2024

extremely difficult to induce methane activation without input of external energy unless such metal atoms cooperate with nonmetal elements (e.g., O,[36] B,[37] and C[38]) or their spin states are elaborately tuned by suitable ligands.[39−41] The exceptions are the clusters composed with the element Ta that Ta_{1-4}^+ cations could dehydrogenate methane at room temperature with high efficiency.[42−44] However, with the further increase of cluster size to Ta_{5-10}^+, only molecular adsorption of CH_4 occurred. The addition of a single or two oxygen atoms to enhance the activity of Ta_4^+, Ta_5^+, and Ta_8^+ were also identified.[45,46] Although detailed mechanisms regarding product formation in methane conversion as well as the modification of local charge distribution of Ta_x^+ by oxygen to promote cluster reactivity have been proposed, the intrinsic electronic origin of the reactivity evolution from small-sized $Ta_{x\le4}^+$ to large-sized $Ta_{x\ge5}^+$ and the critical role of oxygen atoms in tuning the electronic structures of reactive sites are far from clear.

Herein, we systematically investigate the reactivity of a set of $Ta_xO_y^+$ clusters ($x = 2-5$, $y < 2.5x$), totaling 36 species, toward methane by mass spectrometric experiments complemented with theoretical calculations. Note that among the 36 clusters, 6 species including Ta_{2-5}^+ and $Ta_{4,5}O^+$ had been experimentally investigated in literature,[42,44,45,47,48] and the reactivity of the remaining 30 cluster species was newly measured in this work. The localization of σ-bonding electrons in single naked Ta−Ta centers has been emphasized as the root cause of the excellent activity of tantalum clusters displayed in the dehydrogenation of methane at room temperature. The underlying mechanisms for the reactivity evolution from $Ta_{x\le4}^+$ to $Ta_{x\ge5}^+$ as well as the addition of oxygen atoms onto Ta_x^+ to harness the generation and annihilation of localized Ta−Ta σ-type bond and thus modulate cluster reactivity have also been clarified.

2. RESULTS AND DISCUSSION

2.1. Cluster Reactivity

Typical time-of-flight (TOF) mass spectra for the reactions of mass-selected Ta_4^+ and $Ta_4O_{1-5}^+$ clusters with methane at room temperature are shown in Figure 1. It is noteworthy that the reaction systems of $Ta_4O_{2-5}^+$ are newly investigated while the reactivity of Ta_4^+ and Ta_4O^+ that had been previously reported by other research groups[42,43,45] was reexamined for comparison. Upon the interaction of bare Ta_4^+ with 910 mPa CH_4 for about 1.5 ms in our ion funnel trap reactor,[49] the dehydrogenation reaction occurred to produce $Ta_4CH_2^+$ ions (**1**, Figure 1a1). The observation of $Ta_4{}^{13}CH_2^+$ (**1'**, Figure 1b1) in the isotopic labeling experiment with $^{13}CH_4$ further confirmed the reaction channel. Besides the primary reaction, the secondary reaction also took place with $Ta_4C_2H_4^+$ (**3**, Figure 1a1) as a product generated from the dehydrogenation of CH_4 by $Ta_4CH_2^+$, in consistent with the reported results.[42,45] Note that in addition to reaction with CH_4, Ta_4^+ can also interact with the residual water originated from the gas handling system to form Ta_4O^+ (**2**, Figure 1a), which can further dehydrogenate methane giving rise to $Ta_4OCH_2^+$ (**4**), as confirmed by the mass-selection experiments (Figure 1b). Moreover, a higher reactivity of Ta_4O^+ than Ta_4^+ was identified, as evidenced by the stronger relative signal magnitude of $Ta_4OCH_2^+$ than that of $Ta_4CH_2^+$ detected under the experimental conditions with low and high CH_4 pressure, respectively. Such an experimental observation is also

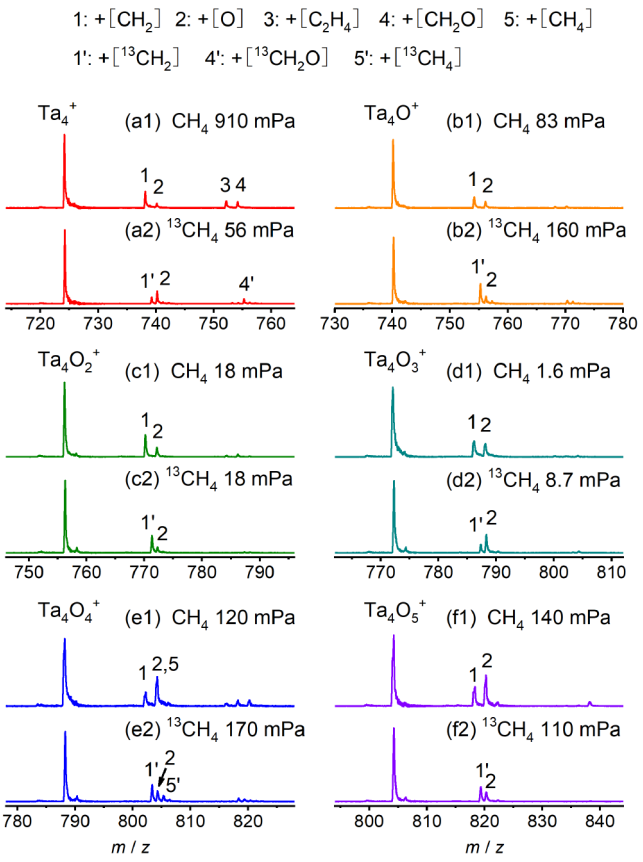

Figure 1. TOF mass spectra for the reactions of Ta_4^+ and $Ta_4O_{1-5}^+$ with CH_4 and $^{13}CH_4$ at room temperature. The pressures of reactant gases pulsed into the ion funnel trap are shown. The reaction time is around 1.5 ms. Peaks assigned as + [O] originated from the reactions of $Ta_4O_y^+$ with water impurities ($Ta_4O_y^+ + H_2O \rightarrow Ta_4O_{y+1}^+ + H_2$) in the ion funnel trap.

in good agreement with the results in literature.[45] With the further addition of oxygen atoms onto Ta_4^+, the cluster reactivity continuously increased such that substantial dehydrogenation product ions could be observed for $Ta_4O_2^+$ and $Ta_4O_3^+$ even extremely low pressure (<20 mPa, Figure 1c,d) of CH_4 was pulsed into the reactor. Although a relatively lower activity of $Ta_4O_4^+$ and $Ta_4O_5^+$ than $Ta_4O_{2,3}^+$ was identified that more than 100 mPa CH_4 should be pulsed in order to evidently observe the $Ta_4O_{4,5}CH_2^-$ product ions (Figure 1e,f), both of them outperformed the bare Ta_4^+. In contrast to bare Ta_4^+ and oxygen-very-deficient clusters $Ta_4O_{y\le5}^+$ that bring about a dehydrogenation reaction with CH_4, the oxygen-less-deficient clusters $Ta_4O_{6-9}^+$ either exhibited inertness or only adsorbed CH_4 without further dehydrogenation (e.g., for $Ta_4O_7^+$).

The variations of reaction channels for $Ta_xO_y^+$ clusters with $x \le 3$ along different numbers of oxygen atoms are strikingly similar to the case of $Ta_4O_y^+$. All of the bare Ta_{2-3}^+ as well as oxygen-very-deficient clusters $Ta_2O_{1,2}^+$ and $Ta_3O_{1-4}^+$ could react with methane to produce $Ta_xCH_2^+$ ions, whereas only CH_4 adsorption was observed for oxygen-less-deficient clusters $Ta_2O_{3,4}^+$ and $Ta_3O_{5-7}^+$ (Table S1). The oxygen-less-deficient clusters in the $Ta_5O_y^+$ series such as $Ta_5O_{6,8-12}^+$ were also found to adsorb CH_4. However, the reactivity variations for $Ta_5O_{0-5}^+$ clusters are quite different from the landscape of oxygen-very-deficient clusters in the $Ta_{x\le4}O_y^+$ series. The

https://doi.org/10.1021/jacsau.4c00032
JACS Au 2024, 4, 1824−1832

monoxide cluster Ta_5O^+ and $Ta_5O_{3-5}^+$ could dehydrogenate methane, but the bare Ta_5^+ and oxide cluster $Ta_5O_2^+$ were unreactive. The superior activity of Ta_5O^+ over Ta_5^+ has also been reported in the literature.[45]

Kinetic analysis of the signal depletion of bare Ta_{2-5}^+ and $Ta_{2-5}O_y^+$ ions as a function of CH_4 pressure was conducted to obtain the rate constants (k_1) with the approximation of a pseudo-first-order reaction mechanism. As shown in Figure 2,

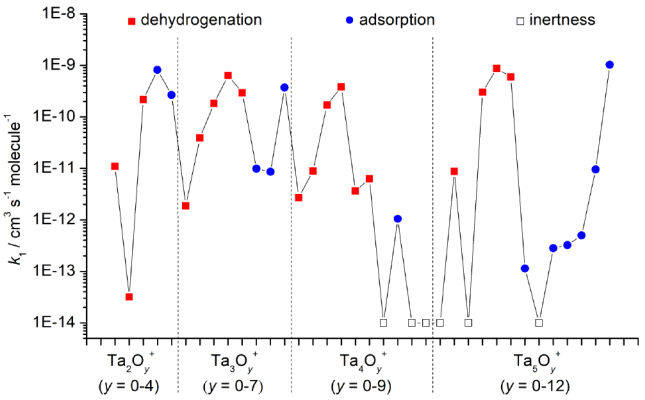

Figure 2. Experimentally determined variation of reaction rates (k_1) for Ta_x^+ clusters and their corresponding oxides $Ta_xO_y^+$ with methane at room temperature. The hollow squares represent the upper limits of k_1.

the k_1 values for the clusters that bring about the dehydrogenation reaction were determined in the range 10^{-12}–10^{-10} cm^3 molecule^{-1} s^{-1} except for Ta_2O^+, for which an extremely low rate on the order of magnitude 10^{-14} cm^3 molecule^{-1} s^{-1} was evaluated. The rates for other clusters with CH_4 adsorption as the sole reaction product vary from 1×10^{-9} to 1×10^{-13} cm^3 molecule^{-1} s^{-1}. For the bare Ta_x^+ reaction systems, the dehydrogenation rates progressively decrease along cluster size (x = 2 → 3 and 4) until no activity is detected when x = 5 under comparable experimental conditions, the variation trend of which is overall consistent with the results reported in literature.[42] Most of the oxide cluster cations were also found to possess significantly larger reaction rates than the corresponding bare Ta_x^+, indicating that oxygen ligands play a crucial role in tuning the activity of tantalum clusters.

In addition to reactions with CH_4, the typical clusters $Ta_4O_y^+$ (y = 0, 1, and 5) interacting with CD_4 were also experimentally investigated (Figure S1). The more intense product peak, which has a mass larger than that of the reactant clusters by 16 au, observed relative to the background signal suggests the occurrence of reactions $Ta_4O_y^+ + CD_4 \rightarrow Ta_4O_yCD_2^+ + D_2$. The estimation of rate constants demonstrates that the dehydrogenation of CD_4 is slower compared to the reactions with CH_4. The kinetic isotope effects (KIE = $k_{1,CH4}/k_{1,CD4}$) were determined to be 9.0 for Ta_4^+, 14.7 for Ta_4O^+, and 4.8 for $Ta_4O_5^+$ (Table S2). The errors (larger than 30%) of KIE values mainly originate from the uncertainty of the rate constants for $Ta_4O_y^+ + CD_4$, which was caused by the signal overlap of background ions $Ta_xO_yO^+$ (generated from the reactions with water impurity in the reactor and gas handling system) and the product ions $Ta_xO_yCD_2^+$. The KIEs for Ta_4^+ and Ta_4O^+ obtained can be comparable to the reported values[45] by considering the experimental uncertainties. The larger KIE value of Ta_4O^+ than that of Ta_4^+ obtained in our study is also in good agreement with the reported results.[45]

2.2. Structures and Reaction Pathways

Density functional theory calculations at the TPSS level[50] were conducted to obtain the cluster structures of Ta_{2-5}^+ and $Ta_{2-5}O_y^+$ (Figures S2 and 3) as well as the reaction pathways between typical clusters and methane. Diatomic Ta_2^+ is electronically stable in the quartet state. When Ta_x^+ upsizes to Ta_{3-5}^+, the lowest-energy geometric configurations evolve from triangles (x = 3) and tetrahedrons (x = 4) to trigonal bipyramids (x = 5), and all of them are stable in the low spin states of triplets or doublets, depending on the clusters composed with odd or even numbers of Ta atoms. The addition of oxygen atoms onto Ta_x^+ clusters could further lower the spin states to render $Ta_xO_y^+$ with x = 3, 5 and x = 2, 4 stable in the singlet or doublet, respectively (except for $^3Ta_5O^+$). Moreover, the configurations of [Ta_x] cores that are originally presented in the bare Ta_{2-4}^+ can be reserved in the $Ta_xO_y^+$ clusters, and the oxygen atoms prefer to be bridgingly bonded (O_b) with the Ta−Ta unit until the [Ta_x] cores are saturated with O_b atoms, such as $Ta_2O_2^+$, $Ta_3O_4^+$, $Ta_4O_6^+$, and $Ta_5O_9^+$ (Figure S2). Other residual O atoms that are necessary to form the oxygen-less-deficient clusters (e.g., $Ta_2O_{3,4}^+$, $Ta_3O_{5-7}^+$, $Ta_4O_{7-9}^+$, and $Ta_5O_{10-12}^+$) are destined to terminally coordinate with different Ta atoms in an energetically preferable sequence.

The Wiberg bond orders (W) for bare Ta_{2-5}^+ and their corresponding oxide clusters have been evaluated by natural bond orbital analysis.[51] The maximum bond order value ($W_{Ta\text{-}Ta}^{max}$) among the Ta−Ta bonds in each cluster is shown in Figure 3 and Table S3. It can be seen that the $W_{Ta\text{-}Ta}^{max}$ overall

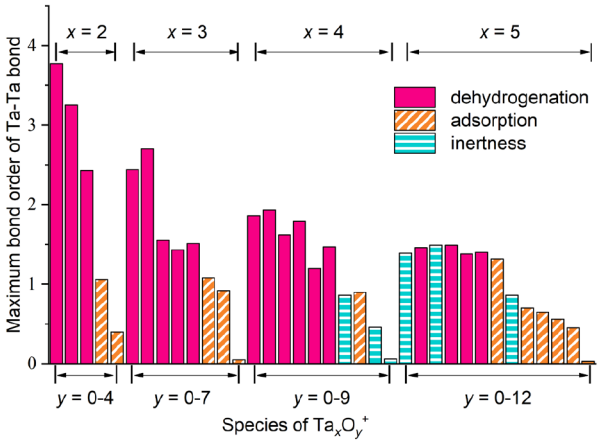

Figure 3. Variation of the maximum bond order values of Ta−Ta in bare Ta_x^+ (x = 2–5) and their corresponding oxides $Ta_xO_y^+$.

progressively decreases as the number of Ta atoms increases, especially for the Ta_x^+ and Ta_xO^+ series. The influence of the number of O atoms on the $W_{Ta\text{-}Ta}^{max}$ values is distinct for different series of $Ta_{2-5}O_y^+$. The gradual increase of O atoms coordinated to Ta_2^+ induces the continuing decline of $W_{Ta\text{-}Ta}^{max}$, whereas an irregular variation of $W_{Ta\text{-}Ta}^{max}$ values along the number of O atoms appears in the case of $Ta_{3-5}O_y^+$. Despite this, a potential commonality connecting the $W_{Ta\text{-}Ta}^{max}$ values to cluster reactivity can be observed that all of the reactive Ta_x^+ and $Ta_xO_y^+$, which can bring about dehydrogenation reaction, have $W_{Ta\text{-}Ta}^{max}$ values located in the range of 1.38–3.77, however,

https://doi.org/10.1021/jacsau.4c00032
JACS Au 2024, 4, 1824−1832

other clusters with $W^{max}_{Ta\text{-}Ta}$ values equal to or smaller than 1.0 are either inert or only reactive toward CH_4 adsorption. The correlation of the bond order of the Ta−Ta bonds to the dehydrogenation activity of $Ta_xO_y^+$ clusters implies that the Ta−Ta bond probably plays an important role in tantalum cluster-mediated methane activation and conversion.

The potential energy profile of the typical reaction mechanism for tantalum clusters that enable methane dehydrogenation is shown in Figure 4. For the tetrahedral

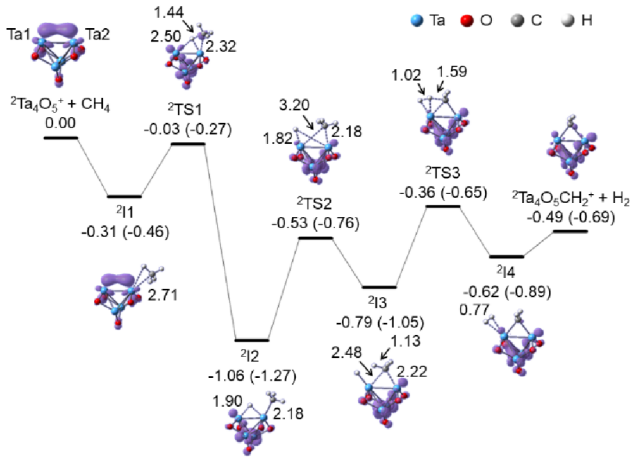

Figure 4. TPSS calculated the potential energy profile for the reaction between the $Ta_4O_5^+$ cluster and CH_4. The superscripts represent the spin multiplicities. The relative energies with zero-point vibration correction (ΔH_0 in eV) and the critical bond lengths (Å) are given. The unpaired spin density distribution for each structure is shown as purple surfaces. The energetic data (ΔH_0) calculated by the method of Zeroth order regular approximation (ZORA),[52,53] with dispersion corrections[54,55] are shown in parentheses.

structure of the $[Ta_4]$ core in $Ta_4O_5^+$, there are six Ta−Ta centers. Each O atom in $Ta_4O_5^+$ is coordinated with one of the Ta−Ta units in the bridging mode, thus, one naked Ta−Ta unit (Ta1−Ta2) with a Wiberg bond order of 1.19 is left out, which could serve as the preferred site to capture and activate CH_4. Either of the equivalent Ta atoms in the naked Ta1−Ta2 can trap the CH_4 molecule to form the encounter complex I1 with a binding energy of 0.31 eV. Then the C−H activation mediated by the cooperation of two Ta atoms proceeds via a transition state that possesses energy lower than that of the separated reactants by 0.03 eV (I1 → TS1). This process leads to the formation of more stable intermediate I2 ($\Delta H_0 = -1.06$ eV) with a Ta2−CH_3 bond and a bridging H atom (H_b) concurrently connected to Ta1 and Ta2. The H_b atom subsequently moves away from Ta2 (I2 → TS2), at the same time, the CH_3 group originally solely bonded by Ta2 also approaches to Ta1 so that the intermediate I3 with Ta1−H and Ta1−CH_3−Ta2 bonds is formed. The

cooperation of Ta1 and the adjacent H atom further drives the CH_2−H bond cleavage (I3 → TS3 → I4). During this step, two H atoms combine to form an H_2 unit that is finally evaporated to produce the most stable ion of $Ta_4O_5CH_2^+$, in which a carbene group is tightly coordinated with Ta1 and Ta2. The reaction intermediates, transition states, and products are all lower in energy than the separated reactants, so the DFT calculations are consistent with the experimental observations. The reaction pathway involving H_3C−H cleavage initiated by Lewis acid−base pair of $Ta^{\delta+}$−$O^{\delta-}$ has also been tested (Figure S3); however, this process was kinetically unfavorable, further confirming the necessity of a cooperative effect between two Ta atoms for methane activation at room temperature. The theoretical rate constants for the reactions of $Ta_4O_5^+$ with CH_4 and CD_4 were calculated (see the detailed methods in Supporting Information), which resulted in a predicted KIE value of 2.8, which can be comparable to the experimental value by considering the experimental and theoretical uncertainties (Table S2).

Similar to $Ta_4O_5^+$, other reactive $Ta_{x\le4}O_y^+$ clusters such as $Ta_4O_{0-4}^+$, $Ta_{2,3}^+$, $Ta_2O_{1,2}^+$, and $Ta_3O_{1-4}^+$ that can dehydrogenate methane identified in experiments also possess naked Ta−Ta bonds and can employ the cooperation of such two adjacent Ta atoms to drive methane activation supported by the energetic data listed in Table S4. In sharp contrast, although there are nine naked Ta−Ta bonds in the Ta_5^+ cluster, the cleavage of the CH_3−H bond initiated by the Ta−Ta center is kinetically unfavorable and is hampered by the positive energy barrier of +0.39 eV (Figure S4), which is in fair agreement with the inert behavior of Ta_5^+ observed in experiments. However, the addition of a single oxygen atom onto Ta_5^+ could significantly lower the reaction barrier to render the [Ta−Ta]-mediated CH_3−H bond cleavage kinetically favorable with a negative barrier (−0.045 eV, Table S4), facilitating the generation of the dehydrogenation product. Other $Ta_xO_y^+$ clusters without naked Ta−Ta bonds were calculated to experience positive enery barriers to break the CH_3−H bond. These computational results thus demonstrate that the naked Ta−Ta bond is the essential site for tantalum clusters to exhibit good activity toward methane, but not all of the naked Ta−Ta bonds could enable CH_3−H cleavage at room temperature. It is noteworthy that the potential energy profiles for the dehydrogenation reactions of $Ta_{4,5}^+$ and $Ta_{4,5}O^+$ with methane have also been investigated in the literature.[45] Although the detailed mechanisms of activating the first C−H bond were not provided, the reaction intermediates with the H and CH_3 fragments bridgingly bonded to two adjacent Ta atoms were located, implying the importance of the cooperative effect between two Ta atoms to promote C−H activation.

2.3. Electronic Origin for the Cluster Reactivity

In order to deeply understand what electronic factors control the activity of Ta−Ta centers toward methane activation, the chemical bonds of Ta_{2-5}^+ and $Ta_{2-5}O_y^+$ were analyzed using the adaptive natural density partitioning (AdNDP) method,[56] which can transform the molecular orbitals into more familiar bonding elements, such as two-center two-electron (2c-2e) bonds or multicenter delocalized bonds. The results demonstrate that all of the Ta_x^+ and $Ta_xO_y^+$ clusters being able to dehydrogenate methane possess localized σ-bonding electrons on single naked Ta−Ta center, however, other less reactive (e.g., $Ta_4O_6^+$ in terms of dehydrogenation reaction) and inert (e.g., Ta_5^+) $Ta_x^+/Ta_xO_y^+$ clusters either possess the available σ-bonding electrons delocalized over multiple Ta−Ta centers or have no such naked Ta−Ta σ-type bond (Figures S5−S7). The typical results for the cluster series of doublets Ta_4^+ and $Ta_4O_y^+$ are presented in Figure 5a. For bare Ta_4^+, there are five 2c−2e and one 2c-1e Ta−Ta σ-type bonds. During the reaction with methane, one of the 2c−2e Ta−Ta bonding σ-type orbitals could facilely interact with the σ^*(C−H) antibonding orbital, ultimately leading to the cleavage of C−H bond. Upon the addition of a single oxygen atom onto Ta_4^+

https://doi.org/10.1021/jacsau.4c00032
JACS Au 2024, 4, 1824−1832

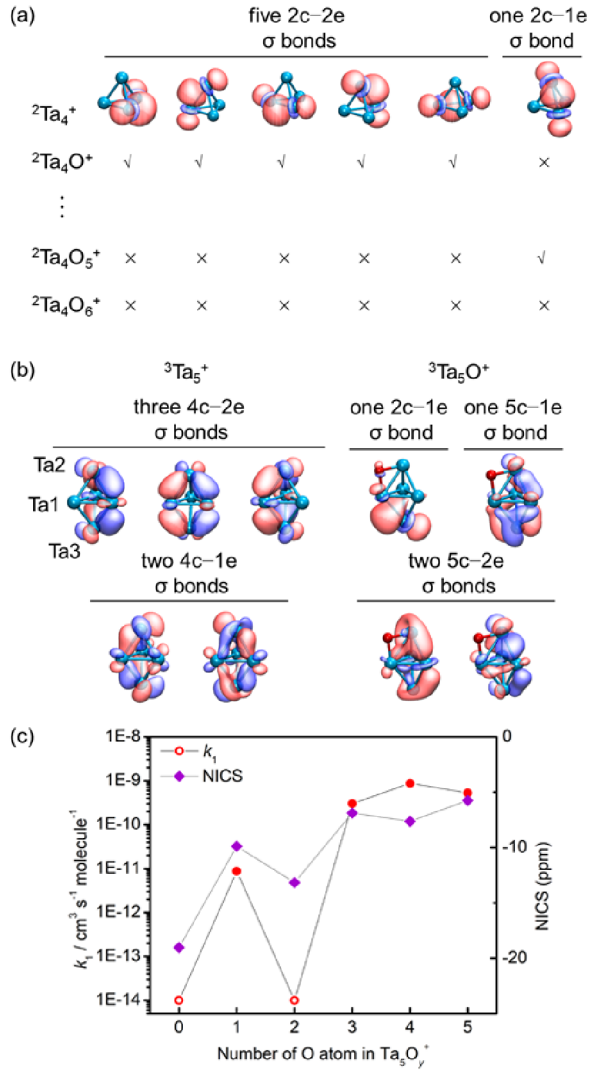

Figure 5. Chemical bonding analysis using AdNDP for $Ta_4O_y^+$ ($y \leq 6$) (a) as well as Ta_5^+ and Ta_5O^+ (b). The correlation of NICS values to the reaction rates for the cluster series of $Ta_5O_y^+$ ($y \leq 5$) is shown in (c).

for the formation of Ta_4O^+, the O atom is bridgingly coordinated to one of Ta−Ta centers and this process inevitably results in the destruction of a localized Ta−Ta σ-type bond. Further oxidation of Ta_4O^+ with additional O_b atoms causes the sequential annihilation of other localized Ta−Ta σ-bonding orbitals until only one 2c−1e Ta−Ta σ-bonding orbital is survived in $Ta_4O_5^+$ (Figure S5). The presence of such localized Ta−Ta σ-bonds renders the activation of the CH_3−H bond by $Ta_4O_{0-5}^+$ kinetically favorable, which lays a solid foundation for the dehydrogenation of methane. Subsequent oxidation of $Ta_4O_5^+$ by atomic oxygen destroys the last remaining Ta−Ta σ-bond and $Ta_4O_6^+$ thus exhibits inertness toward methane, as observed in the experiments. The variation of the localized Ta−Ta σ-type bond from presence to absence found for the $Ta_4O_y^+$ series along the number of oxygen atoms also appears in other cluster series of $Ta_{2,3}O_y^+$ (Figure S6) and strongly correlates with the experimentally observed reactivity. The $Ta_2O_{0-2}^+$ and $Ta_3O_{0-4}^+$ clusters having localized Ta−Ta σ-type bonds could dehydrogenate methane, whereas other clusters without a Ta−Ta σ-type bond, such as $Ta_3O_7^+$, only bring about molecular CH_4-adsorption as a result of electrostatic interaction. It is noteworthy that $Ta_2O_3^+$, $Ta_2O_4^+$, and $Ta_3O_5^+$ clusters, despite the presence of localized Ta−Ta σ-type bond, are also incompetent for the dehydrogenation of methane, attributed to the steric effect of nearby oxygen atoms.

The localized Ta−Ta σ-bond is also an essential reactive center for $Ta_5O_y^+$ to exhibit the dehydrogenation activity, however, the variation trend of Ta−Ta bonding characteristics in the $Ta_5O_y^+$ series is quite distinct from the cases of $Ta_{2-4}O_y^+$. AdNDP analysis revealed that all of the σ-bonding electrons in triplet Ta_5^+ are delocalized over multiple Ta−Ta centers. For example, there are three 4c-2e Ta−Ta σ-type bonds (Figures 5b and S7), each of which involves four Ta atoms interconnected to form a bent rhombic structure (a four-membered ring) that is geometrically advantageous for electron delocalization. The delocalization characteristics of σ-bonding electrons can be further supported by nucleus-independent chemical shift (NICS) analysis along the central axis perpendicular to the planes formed by [Ta_3] units. As shown in Figure 5c, a significant negative NICS value of −27.4 ppm is obtained (corresponding to the point at 1.0 Å above the [Ta_3] plane surface) for Ta_5^+, indicative of the delocalization of σ-electrons over multiple Ta−Ta centers which accounts for the inert behavior of Ta_5^+ toward methane. By contrast, the addition of a single O_b atom onto one of the Ta−Ta centers (such as Ta1−Ta2) in Ta_5^+ could break the electronic environment of bent rhombic structures (two of three), and the delocalization of the σ-electron around such four-membered rings could not happen, thus leading to the localization of the partial σ-electron in the single Ta1−Ta3 center (Figure 5b) that is located adjacent to Ta1−Ta2. The presence of localized Ta−Ta σ-bond in Ta_5O^+ is also reflected by the very small negative NICS value of −1.06 ppm and thus well rationalizes the experimentally observed dehydrogenation activity of Ta_5O^+. Further oxidation of Ta_5O^+ by the second oxygen atom quenches the σ-electron localized in the Ta−Ta bond and finally deactivates $Ta_5O_2^+$ (Figure S7). The localized Ta−Ta σ-type bond could appear again in $Ta_5O_{3-5}^+$ clusters (Figure S7) by destroying the remaining bent rhombic structures in $Ta_5O_2^+$ through additional oxygen atoms, rationalizing the occurrence of a dehydrogenation reaction with methane in the experiments. The less negative NICS values of $Ta_5O_{3-5}^+$ than those of Ta_5^+ and $Ta_5O_2^+$ further support the presence of a localized Ta−Ta σ-bond (note that $Ta_{3,4}^+$ possessing multiple localized Ta−Ta σ-type bonds have positive NICS values, Table S5). The electronic origin for the reactivity variation among $Ta_5O_{0-5}^+$ may provide an insightful understanding on the inferior or superior activity of large-sized Ta_x^+ and $Ta_xO_y^+$ clusters ($x \geq 6$, Table S5).

The delocalization of σ-electrons over multiple Ta−Ta centers in Ta_5^+ and $Ta_5O_2^+$ indicates the aromaticity characteristic of the two clusters.[57] Note that the aforementioned NICS values were obtained by considering the total electrons in Ta_x^+ and $Ta_xO_y^+$. It has been noted that the core electrons of heavy elements have the potential to distort the ring current by creating a strong local circulation.[58] In order to evaluate the effect of core−electron on the NICS values of Ta_x^+ and $Ta_xO_y^+$, the average NICS at the position 1 Å above the center of [Ta_3] planes of Ta_{3-5}^+ and $Ta_5O_{1-5}^+$ have been analyzed by the removal of valence electrons (RVE) approach.[59] We calculated the NICS values of Ta_{3-5}^{n+} and $Ta_5O_{1-5}^{n+}$ (Table S6) without valence electrons at the fixed structures of Ta_{3-5}^+ and $Ta_5O_{1-5}^+$. As a result, the contribution of valence electrons to the NICS values ($NICS_{valence}$) can be

https://doi.org/10.1021/jacsau.4c00032
JACS Au 2024, 4, 1824−1832

obtained by subtracting the core−electron component from the NICS values calculated by considering the total number of electrons ($NICS_{total}$). The $NICS_{valence}$ values are very close to $NICS_{total}$ for Ta_{3-5}^+ as well as Ta_5O^+ and correlate with the relative reaction rates quite well (the clusters with high reactivity possess more positive or less negative NICS values), implying that the effect of heavy metal core−electrons on the NICS of bare and monoxide tantalum clusters is small. However, in the case of $Ta_5O_{2-5}^+$, the $NICS_{valence}$ deviates from $NICS_{total}$ by large values (>3 ppm, Table S6). Further molecular orbital analysis indicates that the core orbitals after removal of the valence electrons of Ta and O atoms are deformed (Figure S8), which may be caused by the narrow energy gap (13.31−13.56 eV) between the lowest occupied orbital of the valence electrons and the highest occupied orbital of the core−electrons for $Ta_5O_{2-5}^+$. It suggests that the RVE approach is not suitable for $Ta_xO_y^+$ clusters to some extent. Despite this, the effect of core−electrons on the NICS of $Ta_5O_{2-5}^+$ clusters can be small according to the results of Ta_{3-5}^+ and Ta_5O^+ from the RVE method.

In order to further explore the role of oxygen atoms played during the process of C−H activation by $Ta_xO_y^+$ clusters, the natural charge analysis was conducted for typical reaction systems of $Ta_4O_y^+$ (y = 0−5) and Ta_5O^+ (Table S7). All of the intermediates I2 formed after activation of the first C−H bond have total charges of the CH_3 moiety and H in the range of −0.57 e ∼ −0.65 e. The electrons accepted by [CH_3, H] in I2 are equal to the charge increase of the reactive Ta−Ta atoms for the reaction systems of Ta_4^+ and $Ta_4O_2^+$. In other reaction systems of Ta_4O^+, $Ta_4O_{3-5}^+$, and Ta_5O^+, the increased total charges of reactive Ta−Ta atoms and other Ta atoms in I2 are almost the same as the accumulated electrons in [CH_3, H], with the reactive Ta−Ta atoms as the dominant electron donors. The results thus indicate that the oxygen atoms in $Ta_4O_y^+$ and Ta_5O^+ behave only as spectators in the course of C−H activation.

Clarifying the electronic features of metal−metal bonds that have the potential to display outstanding activity in bond activation and then establishing of feasible strategies to fine-tune metal−metal interaction are pivotal for the exact design of desirable metal catalysts with dual atoms as reactive sites.[12,16] σ-bond is the basic chemical bond to form substances. Available mechanistic studies about the reactions initiated by metal−metal σ-bonds mainly focused on late transition metals, such as organometallic Pd−Pd[60] and Rh−Rh[61] complexes. The polarized metal−metal σ-bonds formed using early/late heterometals and electronically modified by supporting organic ligands were also frequently reported to be active toward chemical transformations.[12,16,62,63] However, the employment of metal−metal σ-bonds composed of pure early transition metals (ETMs) to activate inert molecules was extremely challenging to achieve[64,65] despite that the oxidative addition reactions initiated by the metal−metal π- or δ-bonds of ETMs (e.g., Mo−Mo and W−W) were known for years.[66−68] In this study, the systematic investigation of the reactivity of ETM clusters Ta_{2-5}^+ and their corresponding oxides (totally 36 species) under isolated gas phase conditions corroborates that the single Ta−Ta center with localized σ-bonding electrons is capable of reducing the C−H bond of the most inert alkane, methane, at room temperature. Changing the geometric configurations (e.g., $Ta_{x\leq4}^+ \rightarrow Ta_5^+$) as well as altering the number of simple inorganic ligands, oxygen atoms, could flexibly manipulate the presence or absence of such a reactive localized Ta−Ta σ-type bond. In order to further understand the activity of the Ta−Ta σ-bond, the activation of C−H bonds in ethane (C_2H_6), propane (C_3H_8), and dimethylbutane (C_6H_{14}) mediated by the Ta−Ta σ-bond in a typical cluster $Ta_4O_5^+$ was also calculated (Figure S9). For reactions with C_3H_8 and C_6H_{14}, the transition states involving secondary and tertiary C−H bond activation are energetically lower than those for activation of the primary C−H bond. Moreover, the relative energies of transition states (activation of the primary or secondary C−H bond) with respect to the separated reactants follow the sequence of $C_6H_{14} < C_3H_8 < C_2H_6 < CH_4$. The results demonstrate that the selectivity for activation of the secondary and tertiary over primary C−H bonds prevails for the reactive site of Ta−Ta σ-bond and that the structuration of the C−H bond dose not limit the reactivity. The mechanistic understanding obtained from C−H activation may also be applicable to the reactivity variations of tantalum clusters toward activation of other inert molecules, such as N_2 and CO_2.[69−71] The strategies discovered for tuning the electron localization of the Ta−Ta σ-bond may be extended to other catalytic systems composed of early transition metals.

3. CONCLUSION

The metal−metal σ-bond composed of early transition metals (Ta−Ta) being able to activate inert chemical bonds (the inert C−H bond of methane) has been identified for the first time by systematic investigation of the reactivity of 36 tantalum clusters. The presence of localized σ-bonding electrons in a single naked Ta−Ta center enables the small-sized clusters Ta_{2-4}^+ to dehydrogenate methane at room temperature; however, the large cluster Ta_5^+ exhibits inertness as a result of the delocalization of σ-bonding electrons over multiple Ta−Ta centers arising from the special geometrical environments (rhombic structures) created by four of the five Ta atoms. The oxygen atoms also play decisive roles in manipulating the presence and absence of a localized Ta−Ta σ-type bond in Ta_{2-5}^+. While the successive addition of oxygen atoms onto Ta_{2-4}^+ gradually annihilates all of the Ta−Ta σ-bonds and ultimately causes the reactivity pattern varying from dehydrogenation to CH_4-adsorption, the coordination of a specific number of oxygen atoms to Ta_5^+ could break the four-membered ring geometrical environments, thus changing the distribution of σ-bonding electrons in Ta−Ta centers from delocalization to localization and finally driving partial $Ta_5O_y^+$ clusters to exhibit dehydrogenation activity. The finding of the unique Ta−Ta center with localized σ-bonding electrons being able to exhibit excellent activity as well as the strategies discovered for tuning the presence or absence of such a reactive Ta−Ta σ-bond provides new routes for the exact design of efficient metal catalysts with a dual atom as reactive sites.

4. METHODS

4.1. Experimental Methods

The positively charged clusters (total 36), including bare Ta_x^+ and oxide $Ta_xO_y^+$ (x = 2−5, $y < 2.5x$), were generated by laser ablation of rotating and translating tantalum foil in the presence of either pure helium (99.9999% purity) or diluted O_2/He (0.01% and 1%) carrier gas with a backing pressure of about 6.0 standard atmospheres. A 532 nm laser (second harmonic of Nd^{3+}:YAG) with an energy of about 5−8 mJ/pulse and a repetition rate of 10 Hz was used. Each of the

https://doi.org/10.1021/jacsau.4c00032
JACS Au 2024, 4, 1824−1832

generated clusters was mass-selected by using a quadrupole mass filter (QMF)[72] and then entered into an ion funnel trap (IFT) reactor,[49] where it was confined and thermalized by collisions with a pulse of He gas for about 0.5 ms. The thermalized Ta_x^+ and $Ta_xO_y^+$ ions reacted with pure or diluted $CH_4/^{13}CH_4$ pulsed into the IFT reactor for about 1.5 ms at room temperature. For the typical clusters of Ta_4^+, Ta_4O^+, and $Ta_4O_5^+$, the reactions with CD_4 were also investigated. The reflection time-of-flight mass spectrometer (TOF-MS)[73] was used to detect the reactant and product cluster cations ejected from the IFT reactor. The details to evaluate the reaction rates can be found in the Supporting Information.

4.2. Theoretical Methods

The density functional theory (DFT) calculations using the Gaussian 16 program[74] were carried out to investigate the structures of Ta_{2-5}^+ and $Ta_{2-5}O_y^+$ as well as the mechanisms of reactions with CH_4. The TPSS functional[50] that had been proven to be suitable for the tantalum cluster systems[64] was employed. The initial structures of small clusters $Ta_2O_{1-3}^+$, $Ta_3O_{0-3}^+$, $Ta_{4,5}^+$, and $Ta_{4,5}O^+$ were obtained by chemical intuition. A Fortran code based on the genetic algorithm[75] was used to search the isomeric structures of relatively large clusters $Ta_2O_4^+$, $Ta_3O_{4-7}^+$, $Ta_4O_{2-9}^+$, and $Ta_5O_{2-12}^+$ with small basis sets (LANL2DZ[76] for all atoms) and coarse convergence thresholds. The low-lying energy isomers obtained were then reoptimized with large basis sets (TZVP[77] for the O atom and def2-TZVP[78] for the Ta atom). Different spin multiplicities for isomers of each cluster were considered to determine the lowest energy structures. The adaptive natural density partitioning (AdNDP) method[56] was used to analyze the chemical bonds of Ta_{2-5}^+ and $Ta_{2-5}O_y^+$ clusters. For $Ta_xO_y^+$ clusters with $x \geq 3$ and $y \geq 0$, the gauge-independent atomic orbital (GIAO) method[79] and the removal of valence electrons (RVE) approach[59] were adopted to calculate the nucleus-independent chemical shift (NICS) values (in ppm) at the points that are 1.0 Å above the planes formed by three Ta atoms along the axis perpendicular to the center of different [Ta_3] surfaces. The reaction mechanism calculations involved the geometry optimization of reaction intermediates (IM) and transition states (TS), through which the IMs transfer to each other. The basis set of TZVP was used for the C and H atoms. The zero-point vibration-corrected energies (ΔH_0, eV) are reported in this work. The Rice−Ramsperger−Kassel−Marcus (RRKM) theory[80] and RRKM-based variational transition state theory (VTST)[80] were used to predict the rates of internal conversion of reaction intermediates. Details on theoretical methods can be found in the Supporting Information.

■ ASSOCIATED CONTENT

Supporting Information

The Supporting Information is available free of charge at https://pubs.acs.org/doi/10.1021/jacsau.4c00032.

Details of experimental and theoretical methods, additional experimental results about product channels and rate data, and additional theoretical results for structural information on tantalum clusters, reaction pathways, bond orders, and NICS values (PDF)

■ AUTHOR INFORMATION

Corresponding Authors

Qing-Yu Liu − *State Key Laboratory for Structural Chemistry of Unstable and Stable Species, Institute of Chemistry, Chinese Academy of Sciences, Beijing 100190, PR China; Beijing National Laboratory for Molecular Sciences and CAS Research/Education Centre of Excellence in Molecular Sciences, Beijing 100190, PR China;* orcid.org/0000-0001-9387-4310; Email: liuqingyu12@iccas.ac.cn

Yan-Xia Zhao − *State Key Laboratory for Structural Chemistry of Unstable and Stable Species, Institute of Chemistry, Chinese Academy of Sciences, Beijing 100190, PR China; Beijing National Laboratory for Molecular Sciences and CAS Research/Education Centre of Excellence in Molecular Sciences, Beijing 100190, PR China;* orcid.org/0000-0002-4425-5211; Email: chemzyx@iccas.ac.cn

Authors

Qian Li − *State Key Laboratory for Structural Chemistry of Unstable and Stable Species, Institute of Chemistry, Chinese Academy of Sciences, Beijing 100190, PR China; University of Chinese Academy of Sciences, Beijing 100049, PR China; Beijing National Laboratory for Molecular Sciences and CAS Research/Education Centre of Excellence in Molecular Sciences, Beijing 100190, PR China*

Sheng-Gui He − *State Key Laboratory for Structural Chemistry of Unstable and Stable Species, Institute of Chemistry, Chinese Academy of Sciences, Beijing 100190, PR China; University of Chinese Academy of Sciences, Beijing 100049, PR China; Beijing National Laboratory for Molecular Sciences and CAS Research/Education Centre of Excellence in Molecular Sciences, Beijing 100190, PR China;* orcid.org/0000-0002-9919-6909

Complete contact information is available at: https://pubs.acs.org/10.1021/jacsau.4c00032

Author Contributions

S.-G.H., Q.-Y.L., and Y.-X.Z. conceived the project. Q.L. conducted the experiments and theoretical calculations. Q.L., Q.-Y.L., and Y.-X.Z. performed data analysis. S.-G.H., Q.L., and Y.-X.Z. contributed to the figures. Y.-X.Z. wrote the manuscript with assistance from all authors. CRediT: **Qian Li** conceptualization, data curation, formal analysis, investigation, visualization, writing-review & editing; **Qing-Yu Liu** conceptualization, data curation, formal analysis, writing-review & editing; **Yan-Xia Zhao** conceptualization, data curation, formal analysis, visualization, writing-original draft, writing-review & editing; **Sheng-Gui He** conceptualization, project administration, supervision.

Notes

The authors declare no competing financial interest.

■ ACKNOWLEDGMENTS

This work was financially supported by the National Natural Science Foundation of China (Nos. 92161205 and 22322307) and the Youth Innovation Promotion Association CAS (Nos. 2018041 and 2022033).

REFERENCES

(1) Dummer, N. F.; Willock, D. J.; He, Q.; Howard, M. J.; Lewis, R. J.; Qi, G.; Taylor, S. H.; Xu, J.; Bethell, D.; Kiely, C. J.; et al.et al. Methane Oxidation to Methanol. *Chem. Rev.* **2023**, *123*, 6359−6411.
(2) Liu, Y.; Wang, R.; Russell, C. K.; Jia, P.; Yao, Y.; Huang, W.; Radosz, M.; Gasem, K. A. M.; Adidharma, H.; Fan, M. Mechanisms for Direct Methane Conversion to Oxygenates at Low Temperature. *Coord. Chem. Rev.* **2022**, *470*, 214691.
(3) Kumar, P.; Al-Attas, T. A.; Hu, J.; Kibria, M. G. Single Atom Catalysts for Selective Methane Oxidation to Oxygenates. *ACS Nano* **2022**, *16*, 8557−8618.
(4) Meng, X.; Cui, X.; Rajan, N. P.; Yu, L.; Deng, D.; Bao, X. Direct Methane Conversion under Mild Condition by Thermo-, Electro-, or Photocatalysis. *Chem* **2019**, *5*, 2296−2325.
(5) Shan, J.; Li, M.; Allard, L. F.; Lee, S.; Flytzani-Stephanopoulos, M. Mild Oxidation of Methane to Methanol or Acetic Acid on Supported Isolated Rhodium Catalysts. *Nature* **2017**, *551*, 605.
(6) Bai, S.; Liu, F.; Huang, B.; Li, F.; Lin, H.; Wu, T.; Sun, M.; Wu, J.; Shao, Q.; Xu, Y.; Huang, X. High-Efficiency Direct Methane Conversion to Oxygenates on a Cerium Dioxide Nanowires Supported Rhodium Single-atom Catalyst. *Nat. Commun.* **2020**, *11* (1), 954.
(7) Luo, L.; Luo, J.; Li, H.; Ren, F.; Zhang, Y.; Liu, A.; Li, W.-X.; Zeng, J. Water Enables Mild Oxidation of Methane to Methanol on Gold Single-atom Catalysts. *Nat. Commun.* **2021**, *12* (1), 1218.
(8) Cui, X.; Li, H.; Wang, Y.; Hu, Y.; Hua, L.; Li, H.; Han, X.; Liu, Q.; Yang, F.; He, L.; et al.et al. Room-Temperature Methane Conversion by Graphene-Confined Single Iron Atoms. *Chem* **2018**, *4*, 1902−1910.
(9) Shen, Q.; Cao, C.; Huang, R.; Zhu, L.; Zhou, X.; Zhang, Q.; Gu, L.; Song, W. Single Chromium Atoms Supported on Titanium Dioxide Nanoparticles for Synergic Catalytic Methane Conversion under Mild Conditions. *Angew. Chem., Int. Ed.* **2020**, *59*, 1216−1219.
(10) Ying, F.; Zhao, B.; Ren, Z.; Xie, J. Graphene-Supported Single-Atom Ni as High-Performance Catalyst for Direct Methane-to-Methanol Conversion. *J. Phys. Chem. C* **2023**, *127*, 19527−19535.
(11) Berry, J. F.; Lu, C. C. Metal−Metal Bonds: From Fundamentals to Applications. *Inorg. Chem.* **2017**, *56*, 7577−7581.
(12) Farley, C. M.; Uyeda, C. Organic Reactions Enabled by Catalytically Active Metal−Metal Bonds. *Trends Chem.* **2019**, *1*, 497−509.
(13) Navarro, M.; Moreno, J. J.; Pérez-Jiménez, M.; Campos, J. Small Molecule Activation with Bimetallic Systems: a Landscape of Cooperative Reactivity. *Chem. Commun.* **2022**, *58*, 11220−11235.
(14) Campos, J. Bimetallic Cooperation across the Periodic Table. *Nat. Rev. Chem.* **2020**, *4*, 696−702.
(15) Luan, Y.-X.; Ye, M. Ligand-Ligated Ni−Al Bimetallic Catalysis for C−H and C−C Bond Activation. *Chem. Commun.* **2022**, *58*, 12260−12273.
(16) Powers, I. G.; Uyeda, C. Metal−Metal Bonds in Catalysis. *ACS Catal.* **2017**, *7*, 936−958.
(17) Wang, Q.; Brooks, S. H.; Liu, T.; Tomson, N. C. Tuning Metal−Metal Interactions for Cooperative Small Molecule Activation. *Chem. Commun.* **2021**, *57*, 2839−2853.
(18) Zhao, Y.-X.; Li, Z.-Y.; Yang, Y.; He, S.-G. Methane Activation by Gas Phase Atomic Clusters. *Acc. Chem. Res.* **2018**, *51*, 2603−2610.
(19) Luo, Z.; Castleman, A. W.; Khanna, S. N. Reactivity of Metal Clusters. *Chem. Rev.* **2016**, *116*, 14456−14492.
(20) Böhme, D. K.; Schwarz, H. Gas-Phase Catalysis by Atomic and Cluster Metal Ions: The Ultimate Single-Site Catalysts. *Angew. Chem., Int. Ed.* **2005**, *44*, 2336−2354.
(21) Lang, S. M.; Bernhardt, T. M. Gas Phase Metal Cluster Model Systems for Heterogeneous Catalysis. *Phys. Chem. Chem. Phys.* **2012**, *14*, 9255−9269.
(22) Schwarz, H. How and Why Do Cluster Size, Charge State, and Ligands Affect the Course of Metal-Mediated Gas-Phase Activation of Methane? *Isr. J. Chem.* **2014**, *54*, 1413−1431.
(23) Yuan, B.; Tang, S.-Y.; Zhou, S. Size Effects in Gas-Phase C−H Activation. *ChemPhyschem* **2023**, *24* (6), No. e202200769.
(24) Wu, H.; Wu, X.-N.; Jin, X.; Zhou, Y.; Li, W.; Ji, C.; Zhou, M. Quadruple C−H Bond Activations of Methane by Dinuclear Rhodium Carbide Cation $[Rh_2C_3]^+$. *JACS Au* **2021**, *1*, 1631−1638.
(25) Roithová, J.; Bakker, J. M. Ion Spectroscopy in Methane Activation. *Mass Spectrom. Rev.* **2022**, *41*, 513−528.
(26) Liu, G.; Zhu, Z.; Ciborowski, S. M.; Ariyarathna, I. R.; Miliordos, E.; Bowen, K. H. Selective Activation of the C−H Bond in Methane by Single Platinum Atomic Anions. *Angew. Chem., Int. Ed.* **2019**, *58*, 7773−7777.
(27) Müller, F.; Stückrath, J. B.; Bischoff, F. A.; Gagliardi, L.; Sauer, J.; Debnath, S.; Jorewitz, M.; Asmis, K. R. Valence and Structure Isomerism of $Al_2FeO_4^+$: Synergy of Spectroscopy and Quantum Chemistry. *J. Am. Chem. Soc.* **2020**, *142*, 18050−18059.
(28) Schwarz, H.; Asmis, K. R. Identification of Active Sites and Structural Characterization of Reactive Ionic Intermediates by Cryogenic Ion Trap Vibrational Spectroscopy. *Chem.—Eur. J.* **2019**, *25*, 2112−2126.
(29) Fayet, P.; Kaldor, A.; Cox, D. M. Palladium Clusters: H_2, D_2, N_2, CH_4, CD_4, C_2H_4, and C_2H_6 Reactivity and D_2 Saturation Studies. *J. Chem. Phys.* **1990**, *92*, 254−261.
(30) Trevor, D. J.; Cox, D. M.; Kaldor, A. Methane Activation on Unsupported Platinum Clusters. *J. Am. Chem. Soc.* **1990**, *112*, 3742−3749.
(31) Ren, Y.; Yang, Y.; Zhao, Y.-X.; He, S.-G. Size-Dependent Reactivity of Rhodium Cluster Anions toward Methane. *J. Phys. Chem. C* **2019**, *123*, 17035−17042.
(32) Nakajima, A.; Kishi, T.; Sone, Y.; Nonose, S.; Kaya, K. Reactivity of Positively Charged Cobalt Cluster Ions with CH_4, N_2, H_2, C_2H_4, and C_2H_2. *Z. Phys. D: At., Mol. Clusters* **1991**, *19*, 385−387.
(33) Liyanage, R.; Zhang, X.-G.; Armentrout, P. B. Activation of Methane by Size-Selected Iron Cluster Cations, $Fe_n^+(n = 2−15)$: Cluster-$CH_x(x = 0−3)$ Bond Energies and Reaction Mechanisms. *J. Chem. Phys.* **2001**, *115*, 9747−9763.
(34) Liu, F.; Zhang, X.-G.; Liyanage, R.; Armentrout, P. B. Methane Activation by Nickel Cluster Cations, Ni_n^+ $(n = 2−16)$: Reaction Mechanisms and Thermochemistry of Cluster-CH_x $(x = 0−3)$ Complexes. *J. Chem. Phys.* **2004**, *121*, 10976−10990.
(35) Lushchikova, O. V.; Reijmer, S.; Armentrout, P. B.; Bakker, J. M. IR Spectroscopic Characterization of Methane Adsorption on Copper Clusters Cu_n^+ $(n = 2−4)$. *J. Am. Soc. Mass Spectrom.* **2022**, *33*, 1393−1400.
(36) Guo, M.; Zhou, S.; Sun, X. Room-Temperature Conversion of Methane to Methanediol by $[FeO_2]^+$. *J. Phys. Chem. Lett.* **2023**, *14*, 1633−1640.
(37) Li, Y.; Wang, M.; Ding, Y.-Q.; Zhao, C.-Y.; Ma, J.-B. Consecutive Methane Activation Mediated by Single Metal Boride Cluster Anions NbB_4^-. *Phys. Chem. Chem. Phys.* **2021**, *23*, 12592−12599.
(38) Geng, C.; Weiske, T.; Li, J.; Shaik, S.; Schwarz, H. Intrinsic Reactivity of Diatomic 3d Transition-Metal Carbides in the Thermal Activation of Methane: Striking Electronic Structure Effects. *J. Am. Chem. Soc.* **2019**, *141*, 599−610.
(39) Zhou, S.; Li, J.; Schlangen, M.; Schwarz, H. Thermal Dehydrogenation of Methane by $[ReN]^+$. *Angew. Chem., Int. Ed.* **2016**, *55*, 14863−14866.
(40) Ma, J.-B.; Xu, L.-L.; Liu, Q.-Y.; He, S.-G. Activation of Methane and Ethane as Mediated by the Triatomic Anion $HNbN^-$: Electronic Structure Similarity with a Pt Atom. *Angew. Chem., Int. Ed.* **2016**, *55*, 4947−4951.
(41) Li, H. F.; Jiang, L. X.; Zhao, Y. X.; Liu, Q. Y.; Zhang, T.; He, S. G. Formation of Acetylene in the Reaction of Methane with Iron Carbide Cluster Anions FeC_3^- under High-Temperature Conditions. *Angew. Chem., Int. Ed.* **2018**, *57*, 2662−2666.
(42) Eckhard, J. F.; Masubuchi, T.; Tschurl, M.; Barnett, R. N.; Landman, U.; Heiz, U. Room-Temperature Methane Activation Mediated by Free Tantalum Cluster Cations: Size-by-Size Reactivity. *J. Phys. Chem. A* **2021**, *125*, 5289−5302.
(43) Lengyel, J.; Levin, N.; Wensink, F. J.; Lushchikova, O. V.; Barnett, R. N.; Landman, U.; Heiz, U.; Bakker, J. M.; Tschurl, M.

https://doi.org/10.1021/jacsau.4c00032
JACS Au 2024, 4, 1824−1832

Carbide Dihydrides: Carbonaceous Species Identified in Ta_4^+-Mediated Methane Dehydrogenation. *Angew. Chem., Int. Ed.* **2020**, *59*, 23631−23635.
(44) Wesendrup, R.; Schwarz, H. Tantalum-Mediated Coupling of Methane and Carbon Dioxide in the Gas Phase. *Angew. Chem., Int. Ed.* **1995**, *34*, 2033−2035.
(45) Eckhard, J. F.; Masubuchi, T.; Tschurl, M.; Barnett, R. N.; Landman, U.; Heiz, U. Thermal Dehydrogenation of Methane Enhanced by μ2-Oxo Ligands in Tantalum Cluster Cations $[Ta_xO]^+$, x = 4, 5. *J. Phys. Chem. C* **2018**, *122*, 25628−25637.
(46) Levin, N.; Lengyel, J.; Eckhard, J. F.; Tschurl, M.; Heiz, U. Catalytic Non-Oxidative Coupling of Methane on $Ta_8O_2^+$. *J. Am. Chem. Soc.* **2020**, *142*, 5862−5869.
(47) Zhou, S.; Li, J.; Schlangen, M.; Schwarz, H. Differences and Commonalities in the Gas-Phase Reactions of Closed-Shell Metal Dioxide Clusters $[MO_2]^+$ (M = V, Nb, and Ta) with Methane. *Chem.—Eur. J* **2016**, *22*, 7225−7228.
(48) Wang, G.; Lai, S.; Chen, M.; Zhou, M. Matrix Isolation Infrared Spectroscopic and Theoretical Studies on the Reactions of Niobium and Tantalum Mono- and Dioxides with Methane. *J. Phys. Chem. A* **2005**, *109*, 9514−9520.
(49) Wei, G.-P.; Liu, Q.-Y.; Ren, Y.; He, S.-G. A ship-lock-type reactor for ion−molecule reactions of mass-selected ions under high-pressure conditions. *Rev. Sci. Instrum.* **2021**, *92* (10), 104104.
(50) Tao, J.; Perdew, J. P.; Staroverov, V. N.; Scuseria, G. E. Climbing the Density Functional Ladder: Nonempirical Meta−Generalized Gradient Approximation Designed for Molecules and Solids. *Phys. Rev. Lett.* **2003**, *91*, 146401.
(51) Glendening, E. D.; Badenhoop, J. K.; Reed, A. E.; Carpenter, J. E.; Bohmann, J. A.; Morales, C. M.; Weinhold, F.*Theoretical Chemistry Institute*; University of Wisconsin: Madison, WI, 2012. http://www.chem.wisc.edu/~nbo5.
(52) Pantazis, D. A.; Chen, X. Y.; Landis, C. R.; Neese, F. All-Electron Scalar Relativistic Basis Sets for Third-Row Transition Metal Atoms. *J. Chem. Theory Comput.* **2008**, *4*, 908.
(53) Weigend, F.; Ahlrichs, R. Balanced basis sets of split valence, triple zeta valence and quadruple zeta valence quality for H to Rn: Design and assessment of accuracy. *Phys. Chem. Chem. Phys.* **2005**, *7*, 3297.
(54) Grimme, S.; Ehrlich, S.; Goerigk, L. Effect of the Damping Function in Dispersion Corrected Density Functional Theory. *J. Comput. Chem.* **2011**, *32*, 1456−1465.
(55) Grimme, S.; Antony, J.; Ehrlich, S.; Krieg, H. A consistent and accurate ab initio parametrization of density functional dispersion correction (DFT-D) for the 94 elements H-Pu. *J. Chem. Phys.* **2010**, *132* (15), 154104.
(56) Zubarev, D. Y.; Boldyrev, A. I. Developing Paradigms of Chemical Bonding: Adaptive Natural Density Partitioning. *Phys. Chem. Chem. Phys.* **2008**, *10*, 5207−5217.
(57) Merino, G.; Solà, M.; Fernández, I.; Nejad, C. F.; Lazzeretti, P.; Frenking, G.; Anderson, H. L.; Sundholm, D.; Cossío, F. P.; Petrukhina, M. A.; Wu, J.; Wu, J. I.; Restrepo, A. Aromaticity: Quo Vadis. *Chem. Sci.* **2023**, *14* (21), 5569−5576.
(58) Periyasamy, G.; Burton, N. A.; Hillier, I. H.; Thomas, J. M. H. Electron Delocalization in the Metallabenzenes: A Computational Analysis of Ring Currents. *J. Phys. Chem. A* **2008**, *112*, 5960−5972.
(59) Orozco-Ic, M.; Charistos, N. D.; Muñoz-Castro, A.; Islas, R.; Sundholm, D.; Merino, G. Core-electron contributions to the molecular magnetic response. *Phys. Chem. Chem. Phys.* **2022**, *24*, 12158−12166.
(60) Fafard, C. M.; Adhikari, D.; Foxman, B. M.; Mindiola, D. J.; Ozerov, O. V. Addition of Ammonia, Water, and Dihydrogen Across a Single Pd−Pd Bond. *J. Am. Chem. Soc.* **2007**, *129*, 10318−10319.
(61) Feng, M.; Chan, K. S. Synthesis and Reactivity of Nonbridged Metal−Metal Bonded Rhodium and Iridium Phenanthroline-Based N_2O_2 Dimers. *Organometallics* **2002**, *21*, 2743−2750.
(62) Karunananda, M. K.; Parmelee, S. R.; Waldhart, G. W.; Mankad, N. P. Experimental and Computational Characterization of the Transition State for C−X Bimetallic Oxidative Addition at a Cu−Fe Reaction Center. *Organometallics* **2015**, *34*, 3857−3864.
(63) Baranger, A. M.; Bergman, R. G. Cooperative Reactivity in the Interactions of X-H Bonds with a Zirconium-Iridium Bridging Imido Complex. *J. Am. Chem. Soc.* **1994**, *116*, 3822−3835.
(64) Li, H.-F.; Zhao, Y.-X.; Yuan, Z.; Liu, Q.-Y.; Li, Z.-Y.; Li, X.-N.; Ning, C.-G.; He, S.-G. Methane Activation by Tantalum Carbide Cluster Anions $Ta_2C_4^-$. *J. Phys. Chem. Lett.* **2017**, *8*, 605−610.
(65) Li, Z.-Y.; Mou, L.-H.; Wei, G.-P.; Ren, Y.; Zhang, M.-Q.; Liu, Q.-Y.; He, S.-G. C-N Coupling in N_2 Fixation by the Ditantalum Carbide Cluster Anions $Ta_2C_4^-$. *Inorg. Chem.* **2019**, *58*, 4701−4705.
(66) Chisholm, M. H. The $\sigma^2\pi^4$ Triple Bond between Molybdenum and Tungsten Atoms: Developing the Chemistry of an Inorganic Functional Group. *Angew. Chem., Int. Ed.* **1986**, *25*, 21−30.
(67) Chisholm, M. H. Interconverting Multiple Bonds between Molybdenum and Tungsten Atoms: Oxidative-Additions and Reductive-Eliminations from Dinuclear Centers. *Polyhedron* **1986**, *5*, 25−30.
(68) Chen, Y.; Sakaki, S. Mo−Mo Quintuple Bond is Highly Reactive in H−H, C−H, and O−H σ-Bond Cleavages Because of the Polarized Electronic Structure in Transition State. *Inorg. Chem.* **2017**, *56*, 4011−4020.
(69) Fries, D. V.; Klein, M. P.; Steiner, A.; Prosenc, M. H.; Niedner-Schatteburg, G. Observation and Mechanism of Cryo N_2 Cleavage by a Tantalum Cluster. *Phys. Chem. Chem. Phys.* **2021**, *23*, 11345−11354.
(70) Levin, N.; Margraf, J. T.; Lengyel, J.; Reuter, K.; Tschurl, M.; Heiz, U. CO_2-Activation by Size-Selected Tantalum Cluster Cations (Ta_{1-16}^+): Thermalization Governing Reaction Selectivity. *Phys. Chem. Chem. Phys.* **2022**, *24*, 2623−2629.
(71) Fries, D. V.; Klein, M. P.; Straßner, A.; Huber, M. E.; Niedner-Schatteburg, G. Cryo-IR Spectroscopy and Cryo-Kinetics of Cluster N_2 Adsorbate Complexes of Tantalum Cluster Cations Ta_{5-8}^+. *J. Chem. Phys.* **2023**, *159* (16), 164306.
(72) Yuan, Z.; Zhao, Y.-X.; Li, X.-N.; He, S.-G. Reactions of $V_4O_{10}^+$ Cluster Ions with Simple Inorganic and Organic Molecules. *Int. J. Mass Spectrom.* **2013**, *354*−*355*, 105−112.
(73) Wu, X.-N.; Xu, B.; Meng, J.-H.; He, S.-G. C−H Bond Activation by Nanosized Scandium Oxide Clusters in Gas-Phase. *Int. J. Mass Spectrom.* **2012**, *310*, 57−64.
(74) Frisch, M. J.; Trucks, G. W.; Schlegel, H. B.; Scuseria, G. E.; Robb, M. A.; Cheeseman, J. R.; Scalmani, G.; Barone, V.; Petersson, G. A.; Nakatsuji, H., et al.et al. *Gaussian 16 Revision C.01*; Gaussian, Inc.: Wallingford, CT, 2016.
(75) Ding, X.-L.; Li, Z.-Y.; Meng, J.-H.; Zhao, Y.-X.; He, S.-G. Density-Functional Global Optimization of $(La_2O_3)_n$ Clusters. *J. Chem. Phys.* **2012**, *137* (21), 214311.
(76) Hay, P. J.; Wadt, W. R. Ab initio Effective Core Potentials for Molecular Calculations. Potentials for K to Au including the Outermost Core Orbitals. *J. Chem. Phys.* **1985**, *82*, 299−310.
(77) Schäfer, A.; Huber, C.; Ahlrichs, R. Fully Optimized Contracted Gaussian Basis Sets of Triple Zeta Valence Quality for Atoms Li to Kr. *J. Chem. Phys.* **1994**, *100*, 5829−5835.
(78) Weigend, F.; Häser, M.; Patzelt, H.; Ahlrichs, R. RI-MP2: Optimized Auxiliary Basis Sets and Demonstration of Efficiency. *Chem. Phys. Lett.* **1998**, *294*, 143−152.
(79) Wolinski, K.; Hinton, J. F.; Pulay, P. Efficient Implementation of the Gauge-Independent Atomic Orbital Method for NMR Chemical Shift Calculations. *J. Am. Chem. Soc.* **1990**, *112* (23), 8251−8260.
(80) Steinfeld, J. I.; Francisco, J. S.; Hase, W. L. *Chemical Kinetics and Dynamics*; Prentice-Hall: Upper Saddle River, NJ, 1999; pp. 231313.

https://doi.org/10.1021/jacsau.4c00032
JACS Au 2024, 4, 1824−1832